Effect of a Wavy Tape Insert and Glass Cover on the Performance of a Photovoltaic Thermal System

Seyed Reza Maadi[1], Hossein Sabzali[1] and David Wood [2]

1 Department of Mechanical Engineering, Ferdowsi University of Mashhad, Mashhad (Iran)

2 Department of Mechanical and Manufacturing Engineering, University of Calgary, Calgary (Canada)

Abstract

Glazed photovoltaic thermal (PV/T) systems compared to unglazed ones provide higher thermal efficiency but reduced electrical efficiency. Thus, to improve the electrical efficiency while keeping the merit of a glazed system, this study equips the PV/T system with a wavy tape insert to augment the heat transfer to the coolant fluid and in turn, reduce the PV cell temperature. This study explores the effect of a wavy tape insert on both glazed and unglazed PV/T systems over the average of selected days in summer at Mashhad, Iran, using computational fluid dynamics. It is found that the insert reduces the PV cell average temperature during the day by 5.9 and 7.1 K for unglazed and glazed modules, respectively, but has a negligible effect on the pump power consumption, which leads to an overall efficiency gain of 11.43% and 13.46% compared to the base case, in that order. Thus, the insert improved the electrical efficiency of glazed PV/T systems, while keeping the merit of the glazed system in increasing the thermal efficiency. The other important issue for solar cells is the temperature distribution within the module which may lead to serious thermal stress and strain. It has been found that using a wavy tape insert can considerably reduce the spatial temperature variation of the cell temperature and consequently improve their lifetime.

Keywords: Glazed photovoltaic thermal system, Unglazed photovoltaic thermal system, mixing devices, Wavy tape insert, computational fluid dynamics, discrete ordinate method.

1. Introduction

Over the years, different studies have been carried out to exploit clean solar energy. The main reasons for these activities are problems such as warming of the earth, rising oil prices, and the predicted end of nonrenewable energy in the near future. International Energy Agency (IEA) predictions on oil supply show that crude oil and petroleum products are expanding, and there will be a decline in crude oil consumption by 2030 (Aleklett et al., 2010). Two of the widespread technologies for utilizing solar energy are photovoltaics (PVs), and solar collector systems, which directly convert sunlight into electricity or thermal energy, respectively. In recent decades PV systems have developed dramatically and, significantly, their cost has reduced (Comello et al., 2018).

According to previous investigations, rising PV plate temperature reduces its electrical conversion efficiency (Skoplaki and Palyvos, 2009). However, a combination of the PV unit and a thermal collector, which is known as a photovoltaic thermal (PV/T) system will reduce the PV cell temperature. Furthermore, fixing a thermal collector below the PV module can increase the PV system lifetime, reduce the installation space, and raise the overall efficiency owing to the utilization of the thermal energy (Moradgholi et al., 2018). Different methodologies have been proposed and developed to improve the performance of PV/T systems, for instance: augmentation of coolant fluid thermophysical properties by using nanofluids (Maadi et al., 2017a; Maadi et al., 2017b), implementation of Phase Change Material (PCM) (Kazemian et al., 2021), an increase in the number of risers in a given total mass flow rate (Maadi et al., 2019c), and employing a thermoelectric device in the system (Kolahan et al., 2020).

One of the methods for increasing heat transfer in many applications is to insert mixing devices in the collector tubes, but these are rarely used in photovoltaic thermal (PV/T) systems. Using such devices in parabolic trough collectors (PTCs) can increase heat transfer about 20-300%, and 10-200%, for the laminar and turbulent regime, in that order (Sandeep and Arunachala, 2017). As their name implies, mixing devices increase mixing and in turn increase in the heat transfer rate (Jaisankar et al., 2011). The price paid is an increase in the pressure drop, which means more pump power is needed (Bellos et al., 2017) and must be considered in optimizing the thermal

performance. Recently, Maadi et al. (2020) scrutinized the effect of conical-leaf inserts in different geometrical parameters and various operating conditions on the performance of an unglazed PV/T system. The inserts reduced the cell temperature by up to 7 K, which, in turn, lead to considerable improvement in electrical and thermal efficiencies. Moreover, it has been found that the pump power was negligible compared to the electrical output power. In another study by Maadi et al. (2021), the effect of a wavy-tape insert along with Al_2O_3-water nanofluid for an unglazed PV/T system was examined. A tube equipped with a wavy-strip insert, and a nanofluid with a volume fraction of 3% improved the thermal and electrical efficiencies by 12.06% and 3.5% compared to a water-based PV/T module with the bare tube, respectively.

Another method to increase thermal efficiency is trapping the light by using one or more glass covers. Installation of a glazed cover above the PV/T system (Glazed PV/T system) on the one hand reduces the total heat transfer loss to the surroundings, which increases the thermal efficiency of the system. On the other hand, the electrical efficiency reduces as the cells experience higher temperature, and a portion of incident solar irradiation is reflected from the cell surface and is absorbed by the glass cover (Chow et al., 2009; Kazemian et al., 2018).

Based on the literature review, using an insert in the coolant tube can lead to a considerable improvement of the tube's heat absorption rate. The use of mixing devices has advantages such as: ease of installation and removal from a bare tube, a negligible effect on the strength of the original tube, and cheapness. Nevertheless, there is little knowledge of the integration of mixing devices with PV/T modules to increase their performance. To this end, this study investigates the effect of a glass cover and a wavy tape insert simultaneously on the performance of the PV/T module. A 3D model is presented with the simulation of the entire layers of the PV/T system along with thermophysical and optical properties. For simulating the optical behavior of different components of the PV/T module, the discrete ordinate (DO) method, along with the solar ray tracing algorithm, is employed. Furthermore, the proposed simulation has sufficient accuracy to capture the exchange of short to long-wavelength radiation in the air gap between the glass cover and the surface of the PV cells. In other words, by using the two-band radiation DO model, the greenhouse effect is considered. According to the literature review, this is the first time the proposed simulation is taken into account for comparing the glazed and unglazed PV/T systems.

2. Numerical simulation

The governing equations for modeling the fluid in steady state, are as follows.

Continuity:
$$\vec{\nabla}.\left(\rho_f \vec{V}_f\right) = 0 \qquad \text{(eq. 1)}$$

Momentum:
$$\vec{\nabla}.\left(\rho_f \vec{V}_f \vec{V}_f\right) = -\vec{\nabla}P_f + \vec{\nabla}.\tau_1 + \rho_f \vec{g} \qquad \text{(eq. 2)}$$

Energy:
$$\vec{\nabla}.\left(\rho_f C_{p.f} T_f \vec{V}_f\right) = \vec{\nabla}.\left(k_f \vec{\nabla}T_f\right) \qquad \text{(eq. 3)}$$

where $\rho, \vec{V}, P, \tau_1, C_p, T$, g, and k are density, velocity, pressure, shear stress, specific heat capacity, temperature, gravity, and thermal conductivity, respectively. Subscript f specifies the fluid (air or water). For the glazed PV/T module, as shown in Fig. 1, there is free convection inside the gap, which is simulated with the Boussinesq approximation. In this model, density is considered constant in all governing equations except for the buoyancy term in the momentum equation (Maadi et al., 2019b):

$$(\rho_{air} - \rho_{amb})g \approx -\rho_{amb}\beta(T - T_{amb})g \qquad \text{(eq. 4)}$$

In (eq. 4), in order, ρ_{amb}, and β refer to the air density at the ambient temperature (T_{amb}) and the thermal expansion coefficient. The formula for solving the conduction heat transfer in solid part is (Maadi et al., 2019b):

$$k_s \nabla^2(T_s) - \gamma e'_{elec} + S_h = 0 \qquad \text{(eq. 5)}$$

where γ is the constant coefficient, equal to one for the PV cells, and zero for the remaining solid parts. The subscript s refers to the solid layers. The second term in (eq. 5) indicates the output of electrical power per unit volume of the PV cells. The electrical power of the PV cells is derived from a well known relation (Skoplaki and Palyvos, 2009):

$$E_{elec} = \dot{S}\,\eta_{ref}(1\text{-}\beta_{ref}\,(T_{PV} - T_{\text{ref}}))\,P_a \qquad \text{(eq. 6)}$$

where, β_{ref}, T_{ref}, η_{ref}, and T_{PV} are reference temperature coefficient, reference temperature, reference cell efficiency, and PV cell temperature respectively. P_a is called the packing factor, which is the ratio of the area of the solar cells to the PV module area (Skoplaki and Palyvos, 2009). In (eq. 6), $\dot{S}$ denotes the effective absorbed solar irradiance by the solar cells, and is given by (Maadi et al., 2019b) as

$$\dot{S} = \tau_g\,\bar{\alpha}_{PV}\,G_{sun} \qquad \text{(eq. 7)}$$

where, τ_g, $\bar{\alpha}_{PV}$, and G_{sun} are glass transmittance, the effective absorptance of PV cells, and incident solar radiation, respectively.

Fig. 1 elaborates the main heat transfer mechanisms in both glazed and unglazed PV/T systems. The glass cover has different transparency at different light wavelengths. In other words, it has spectral optical properties. For the long-wavelength region it is almost opaque, while for the remaining wavelengths, it is semi-transparent. Therefore, according to Fig. 1 for the glazed PV/T system, the short spectrum irradiation passes through the glass cover and is incident on the PV cells ($G_{t,g}$). Some part of it is absorbed by the cells ($G_{a,PV}$), and the remainder reflects as a long wavelength ($G_{r,PV}$) (Maadi et al., 2019b). As shown in the figure, most of this reflected light is trapped inside the gap zone and gives rise to the greenhouse effect (Maadi et al., 2019b). The greenhouse effect is one of the essential differences between the glazed and unglazed systems. As clearly seen in Fig. 1, the glass cover results in a portion of solar irradiance being reflected to the surrounding ($G_{r,g}$), and a very small amount of it is absorbed by the glass cover ($G_{a,g}$); hence, in contrast to the unglazed one, less solar irradiance reaches the cells. Moreover, in the glazed PV/T system compared to the unglazed one, the thermal energy loss to the surrounding is reduced. In Fig. 1 q_{rad} refers to the thermal radiation either in the gap or to the surrounding, and q_{conv} refers to the forced convection of the exterior surface.
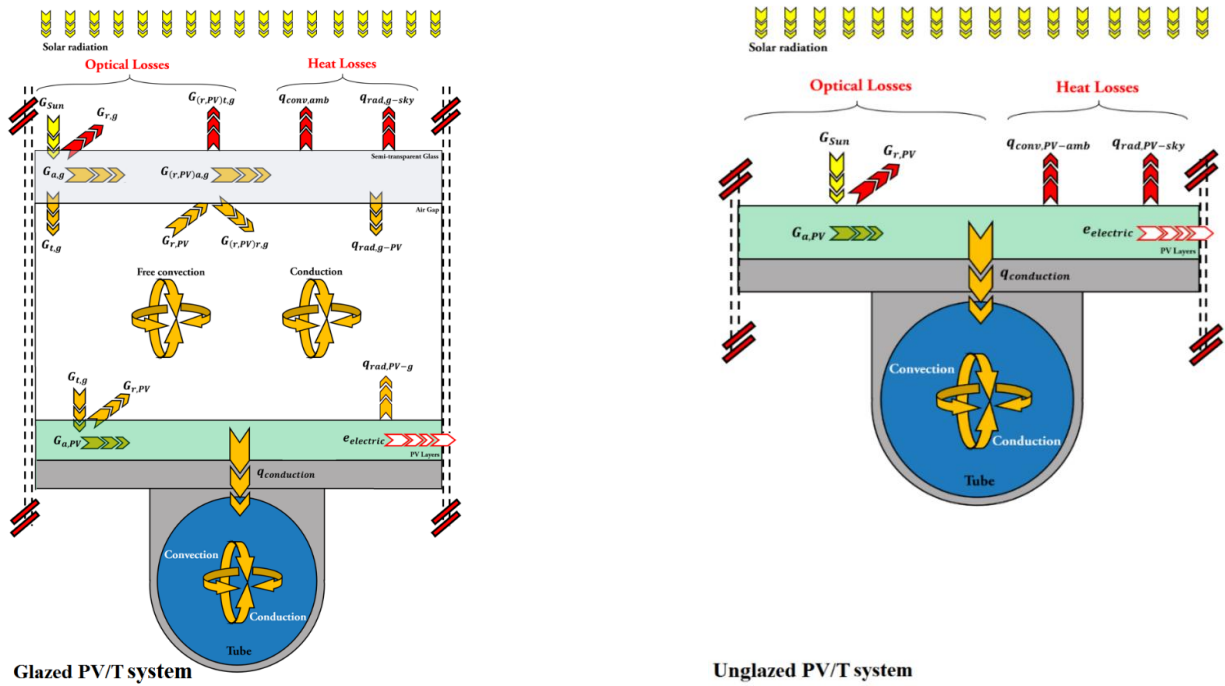

Fig. 1: The main heat transfer mechanisms in both glazed and unglazed PV/T modules.

For simulating the optical behavior of different components of the PV/T module, the DO technique, along with

the solar ray tracing algorithm, is employed. Furthermore, the simulation has sufficient accuracy in simulating the exchange of short wavelength to long wavelength radiations to capture the greenhouse effect. Further information is provided in the study of Maadi et al. (2019b).

In (eq. 5), S_h is a heat source due to the incident solar irradiance absorbed by the solid layers shown in Fig. 2. For the glazed PV/T system, S_h is determined by the Radiative Transfer Equation (RTE), along with solar ray tracing, which simultaneously solves the continuity, momentum, and energy equations. In this study, the DO radiation model is adopted to solve the RTE for a finite number of discrete solid angles, each related with a vector direction fixed in the global Cartesian system (x, y, z). Further information is given by (Modest, 2013).

In order to model the wavelength-dependent optical properties, the RTE for the spectral intensity $I_\lambda(\vec{r}.\vec{s})$ must employ non-gray radiation at position $\vec{r}$ in the direction $\vec{s}$, which is derived as (Maadi et al., 2019b):

$$\vec{\nabla}.(I_\lambda(\vec{r}.\vec{s})\vec{s}) + (\sigma_\lambda + \sigma_s)I_\lambda(\vec{r}.\vec{s}) = \sigma_\lambda n^2 I_{b\lambda} + \frac{\sigma_s}{4\pi}\int_0^{4\pi} I_\lambda(\vec{r}.\vec{s})\Phi(\vec{s}.\vec{s}')d\Omega' \qquad \text{(eq. 8)}$$

where σ_λ, $\vec{s'}$, σ_s, Ω', Φ, n, and $I_{b\lambda}$ are spectral absorption coefficient, scattering direction vector, scattering coefficient, solid angle, phase function, refractive index, and the blackbody intensity which is given by the Planck function, respectively. Furthermore, $(\sigma_\lambda + \sigma_s)$ denotes the optical thickness or capacity of the medium. The total intensity $I_\lambda(\vec{r}.\vec{s})$ in every direction of $\vec{s}$ at position $\vec{r}$ over the wavelength regions is calculated by summation of over each wavelength band as (Maadi et al., 2019b):

$$I_\lambda(\vec{r}.\vec{s}) = \sum_k I_{\lambda_k}(\vec{r}.\vec{s})\,\Delta\lambda_k \qquad \text{(eq. 9)}$$

In (eq. 9) for each band, the optical properties are considered as wavelength-independent (gray). The black body emission over each wavelength interval per unit solid angle evaluated as (Maadi et al., 2019b):

$$E_b(\lambda.T) = [F(0 \to n\lambda_2 T) - F(0 \to n\lambda_1 T)]n^2\frac{\sigma T^4}{\pi} \qquad \text{(eq. 10)}$$

In (eq. 10) according to the Planck distribution, $F(0 \to n\lambda T)$ is the ratio of radiant energy of a black body over the wavelength interval from 0 to λ at temperature T emitted in a medium with the refractive index *n*.

Since the PV cells are opaque, the radiation incident in each band on the surface is calculated as (Maadi et al., 2019b):

$$\dot{q}_{inc.PV.\lambda} = \Delta\lambda \int I_{in.\lambda}\vec{s}.\vec{n}d\Omega \qquad \text{(eq. 11)}$$

and net radiative energy flux at each wavelength from the PV cells surface is derived as (Maadi et al., 2019b):

$$\dot{q}_{out.PV.\lambda} = (1 - \varepsilon_{PV.\lambda})q_{PV.inc.\lambda} + \varepsilon_{PV.\lambda}[F(0 \to n\lambda_2 T) - F(0 \to n\lambda_1 T)]n^2\sigma T_{PV}{}^4 \qquad \text{(eq. 12)}$$

where $\varepsilon_{PV.\lambda}$ and σ are the PV cells emissivity in each band, and the Stefan-Boltzmann constant equal to $5.67 \times 10^{-8}\,W/m^2K^4$, respectively.

Fig. 2 demonstrates the schematic of the proposed PV/T system along with its boundary conditions and components. In this study, we considered a PV/T module with five straight tubes, *N*=5 of diameter 0.05m. The entire characteristics of the simulated PV/T system are presented in Tab. 1 and thermophysical properties of different components can be found in the study of Maadi et al. (2020), and their optical properties were given in the study of Maadi et al. (2019a). In this study, the PV/T module without a glass cover and using the plain tube is called the base case, and the effect of the wavy tape insert and glass cover on the PV/T efficiencies are compared with it.

Tab. 1: characteristics of the simulated PV/T system (Bhattarai et al., 2012; Khanjari et al., 2016; Lu and Yao, 2007)

Component	Parameter	Definition	Value	Unit
Glass cover	t_g	Glass thickness	0.004	m
Air gap	$t_{air\text{-}gap}$	Air gap thickness	0.012	m
Encapsulated Si	L	Length	2	m
	W	Width	1.5	m
	t_{eva}	EVA layer thickness	0.0005	m
	t_{arc}	ARC layer thickness	8×10^{-8}	m
	t_{si}	Si layer thickness	0.0003	m
	t_{tedlar}	Tedlar layer thickness	0.0001	m
Absorber plate	t_{abs}	Absorber layer thickness	0.002	m
Tube	D	Diameter	0.05	m
	t_t	Tube thickness	0.003	m
	N	Number of tubes	5	-
	S	Space between tubes	0.3	m

In this study, pure water is the coolant and its thermophysical properties are temperature-dependent (Maadi et al., 2019a). For evaluating the thermal radiation, the external radiation temperature is considered as sky temperature, which depends on the ambient temperature [59] according to

$$T_{sky} = 0.0552 T_{amb}^{1.5}. \qquad \text{(eq. 13)}$$

For calculating the forced convection, the convective heat transfer coefficient is obtained by (eq. 14) [7].

$$h_{wind} = 2.8 + 3V_{wind} \qquad \text{(eq. 14)}$$
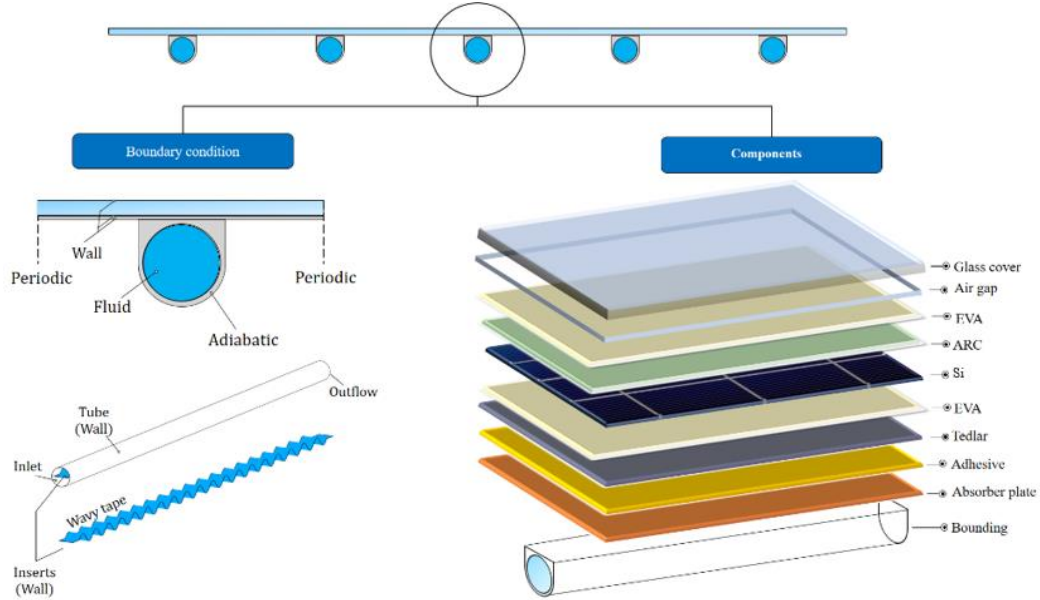
where V_{wind} is the local wind speed.

Fig. 2: Front view schematic of the proposed typical PV/T system along with its boundary conditions and perspective 3D view of the tube along with considered wavy tape insert.

2.1 Performance evaluation

For evaluating the performance of the PV/T module, we consider the thermal efficiency (η_{th}), electrical efficiency (η_{elec}), and overall efficiency (η_{ov}), defined as

$$\eta_{th} = \frac{\dot{m} C_{p.w}(T_{W.out} - T_{W.in})}{A G_{sun}} \qquad \text{(eq. 15)}$$

$$\eta_{elec} = \frac{E_{elec} - E_{pump}}{AG_{sun}} \qquad \text{(eq. 16)}$$

$$\eta_{ov} = \eta_{th} + \eta_{elec} \qquad \text{(eq. 17)}$$

In (eq. 15), in order, $\dot{m}, C_{p.w}, A, T_{W.out}$ and $T_{W.in}$ refer to the inlet mass flow rate, water specific heat, module area, outlet, and inlet water temperature inside the tube. In (eq. 16), E_{pump} is the pump power consumption, which is calculated as (Maadi et al., 2019b):

$$E_{pump} = \frac{N\dot{m}\Delta\text{p}}{\rho_w \eta_{pump}} \qquad \text{(eq. 18)}$$

where, in order Δp, and η_{pump} are the pressure drop in one tube, and pump efficiency. The pump efficiency is assumed to be 0.8 (Maadi et al., 2019a).

2.2 Grid independency

Fig. 3-a shows the 3D meshes. In order to balance the independence of the results from the size of the grids, against the execution time, different element numbers are examined. Outlet temperature and PV cell temperature are considered as the criteria to investigate grid independence. As illustrated in Fig. 3-b for the unglazed PV/T systems, by increasing the number of elements from grid 3 to 4, for both the plain tube and tube with a wavy tape, the outlet temperature and PV cell temperature remain constant. Therefore, we selected grid 3 with 800000 cells for the bare tube and 1600000 cells for the tube with a wavy tape, for the remainder of this study. Moreover, for the glazed PV/T system, the glass and gap layers required160000 more elements above the PV cells.

In the optical simulation, overall directions of $N_\theta \times N_\Phi$ per wavelength band are solved. For three-dimensional calculations, a total number of $8 \times N_\theta \times N_\Phi$ directions of the RTE equation are calculated. These control angles are then discretized by pixelation. Maadi et al. (2019b) recommended a pixelation and a division of 3×3 for a semi-transparent material. These values were used here.
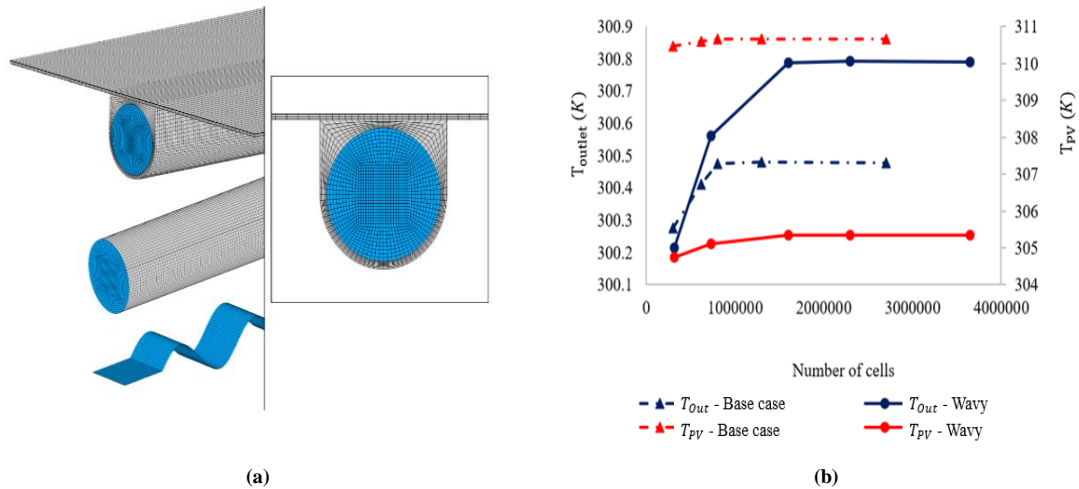

(a)   **(b)**

Fig. 3: (a) the schematic of the grid for typical PV/T module and the insert tape (b) grid independence of the base case with and without wavy tape insert

2.3. Validation:

To verify the accuracy of the solution, the numerical data are validated with those available experimental data of the typical PV/T module (Bhattarai et al., 2012). The comparison is performed for the outlet and PV plate temperatures. As is depicted in Fig. 4, an average error below 3.8% and 4.9% in order, for electrical efficiency and thermal efficiency is obtained. Therefore, the proposed numerical model has sufficient accuracy in modeling optical and thermal performance.
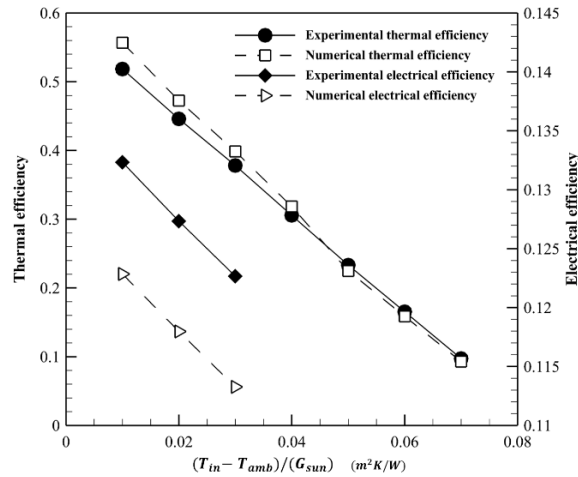
Fig. 4: Validation of the current numerical model with experimental data of thermal and electrical efficiencies of the PV/T module.

3. Results and discussion

The wavy tape insert in the current study is the optimal configuration of Zhu et al. (2016). The evaluation is done on the average daily variation on selected days in summer at Mashhad, Iran (see Fig. 5) (Sardarabadi et al., 2017). Fig. 6 shows the daily variation of T_{out} and the T_{PV} for the base case, and both glazed and unglazed PV/T systems with wavy tape insert. This figure reveals that encapsulating a PV/T system with a glass cover increases the T_{out} and the T_{PV}; however, at the beginning and end of the day when the insolation is low, the glass cover has little effect on the system temperature. The figure shows the insert reduces the mean T_{PV} during the day by 5.9 and 7.1 K for unglazed and glazed modules, respectively, and in turn, increases T_{out}. The reduction in the T_{PV} is more pronounced during peak insolation (hour 13:00), with a 6.8 and 8.2 K decrease for unglazed and glazed PV/T systems, respectively. The results demonstrate the pump power to the PV plate electrical output power, that is E_{Pump}/E_{elec}, for all cases is less than 0.0001%, which is negligibly small. Fig. 7 demonstrates the average overall loss, thermal, and electrical efficiencies over the day for the three systems. A large portion of the incoming solar radiation is wasted, but the wavy tape insert considerably reduces the loss for an unglazed PV/T system by about 65%; while, encapsulating the PV/T system with a glass cover reduces the loss by 86%, due to the light trapping. As shown in Fig. 7, using a wavy tape insert improves the η_{th} for glazed and unglazed PV/T systems by 17.32%, and 13.06%, respectively. In terms of η_{elec}, this improvement is equal to 3.46% for the unglazed PV/T system; while, it can be seen that for the glazed PV/T system despite the insert, the η_{elec} is reduced by 5.3% compared to the base case. Indeed, for the glazed case, only 93% of the solar irradiance is transmitted through the glass cover and strikes by the PV cells, which means 7% of G_{sun} is lost and this causes the lower η_{elec} compared to the base case. Thus the additional cost and weight of the glass cover is combined with a lower η_{elec}, which can be counteracted by extracting further heat from the PV module to the coolant fluid. In terms of η_{ov}, the glazed PV/T system provides higher η_{ov}, and using the insert improves the unglazed and glazed PV/T modules by 11.43% and 13.46% compared to the base case, respectively.
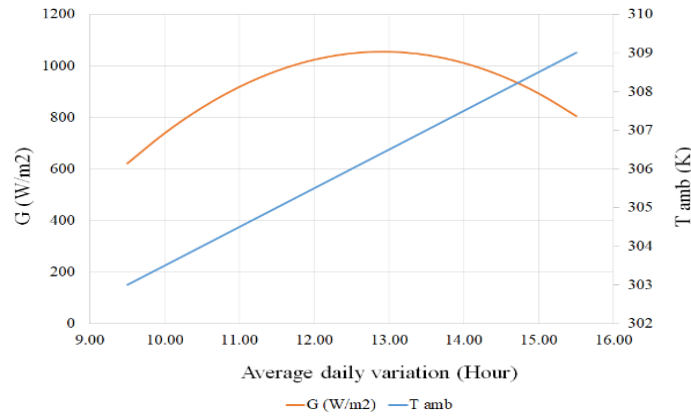
Fig. 5: Average daily variation of G_{sun} and T_{amb} on typical days in August and September at Mashhad, Iran (Sardarabadi et al., 2017)
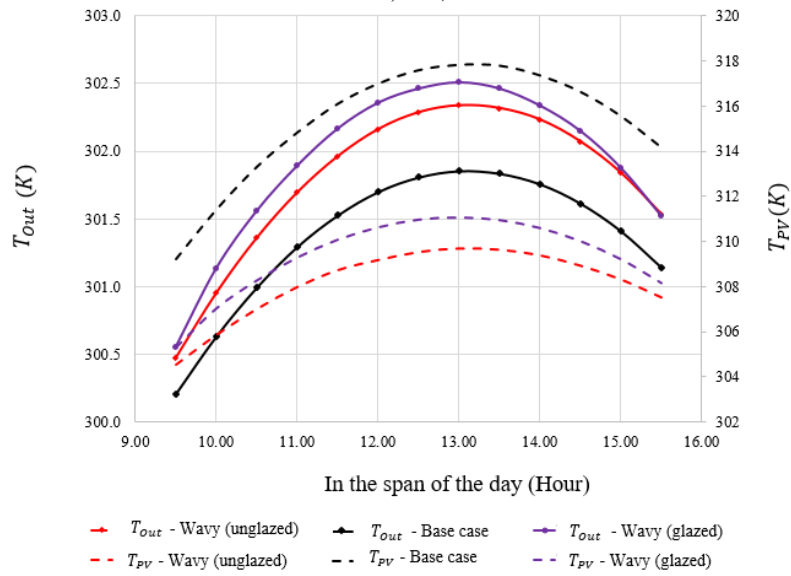

Fig. 6: Daily variation of outlet temperature and the PV temperature of the collector for the base case and both glazed and unglazed PV/T system integrated with wavy tape insert
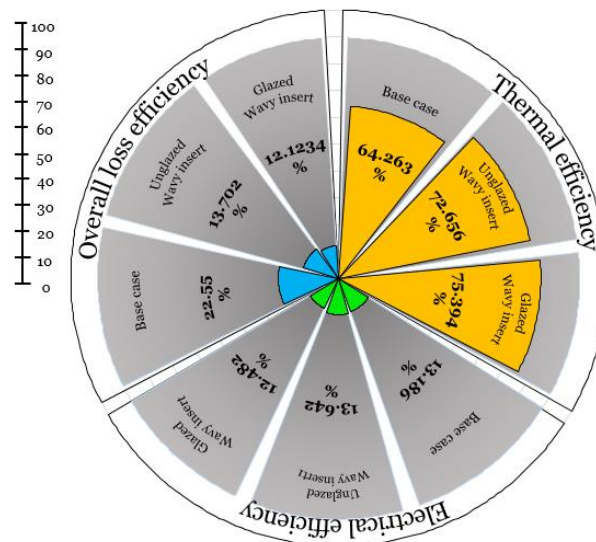

Fig. 7: Comparison of the share of thermal, electrical, and overall loss efficiencies for the base case and both glazed and unglazed PV/T system integrated with wavy tape insert

The temperature distribution on the PV cells may lead to crucial thermal stresses, which in turn cause serious problems such as fractured cells, broken interconnections, reduction of cell power, and as well as lifetime

reduction. Fig. 7 illustrates the effect of the insert on the spatial variation of T_{PV} at three different hours 9:30, 12:30, and 15:30. As can be seen, the insert strikingly reduces the temperature gradient particularly around the peak insolation hour, 12:30. Fig. 8 shows the maximum temperature difference on the PV unit at the three different hours of the day. The insert reduces the maximum temperature difference, in order, for glazed and unglazed PV/T systems by 4.17 and 4.47 K at 9:30, 7.01, and 7.65 K at 12:30, and 6.2 and 6.46 K at 15:30. Therefore, the biggest reduction in thermal stress is obtained at the peak insolation.

(a) 9:30
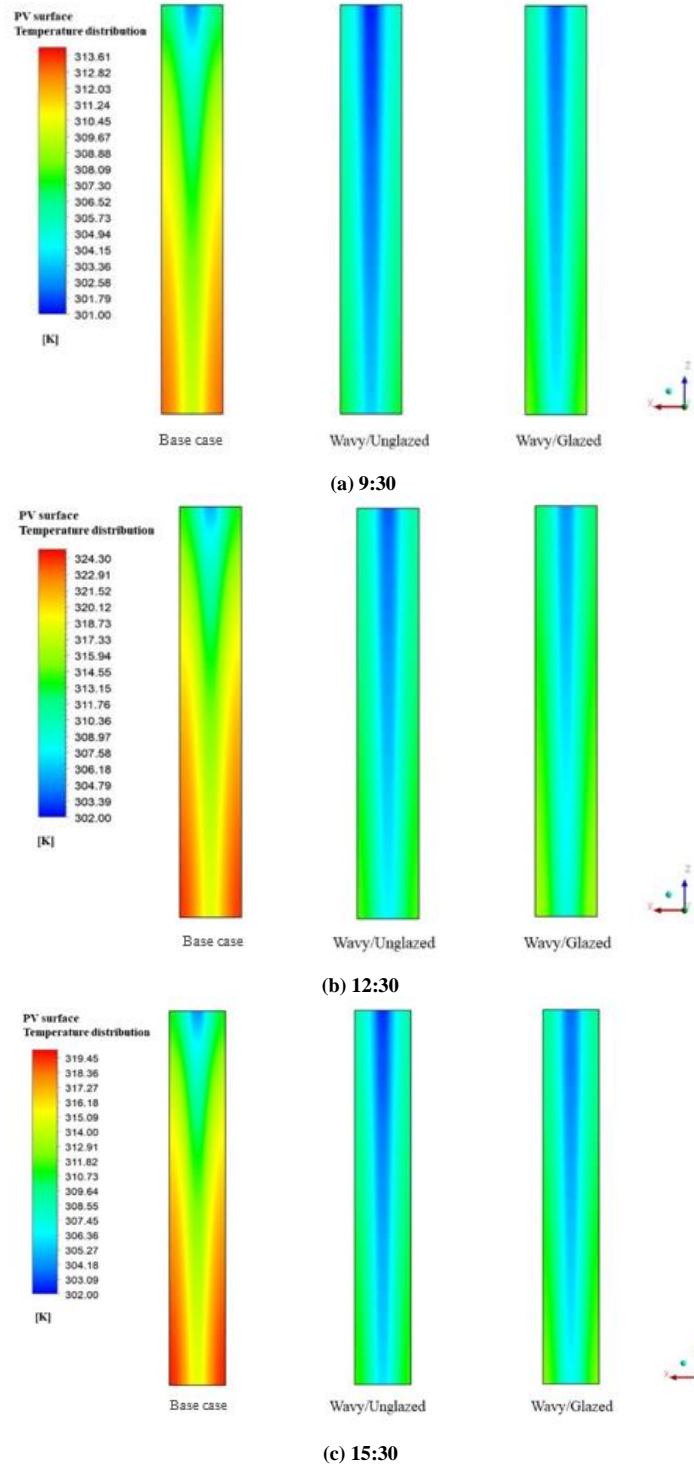
(b) 12:30

(c) 15:30

Fig. 8: Surface temperature distribution of the PV cell at three different hours of the day at a) 9:30 b) 12:30 c) 15:30. The figures show the central one-fifth of the module with the coolant tube in the middle.
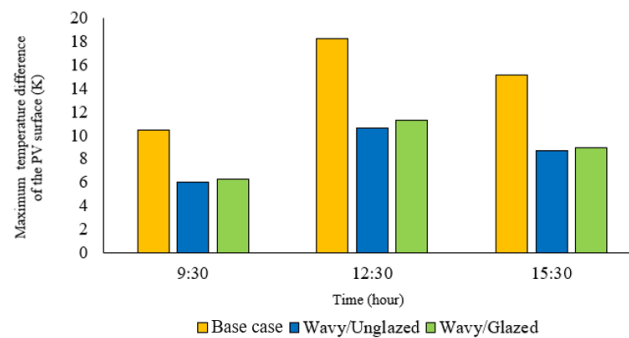
Fig. 9: Maximum temperature difference of the PV surface at three hours of the day

4. Conclusions

This numerical study considered the interaction of thermal and electrical performance of three photovoltaic/thermal (PV/T) systems: an unglazed PV/T system with the plain thermal collector tube (base case), a PV/T with a wavy tape insert for the glazed, and unglazed PV/T systems. A tube fitted with a wavy tape insert showed a reduction of PV cell temperature of the glazed PV/T system while keeping the merit of the glazed system in increasing the thermal efficiency. Using the insert reduces the average PV cell temperature during the day by 5.9 and 7.1 K for unglazed and glazed modules, respectively, and in turn, suppressing the energy losses by 65% and 86%, in that order. The reduction in PV cell temperature is more pronounced during peak insolation (hour 12:30). As 7% of the solar irradiance transmitted through the glass cover does not reach the PV plate, the electrical efficiency of the glazed PV/T system is lower than the base case. The reduction of the light incident on the PV plate lowers the electrical efficiency more than the reduction of the PV plate temperature caused by the insert in the collector tube which increases the electrical efficiency. It is worth mentioning the pump power is negligible compared to the PV plate's electrical output power. The results show that a wavy tape insert compared to the base PV/T system improves the thermal efficiency for glazed and unglazed PV/T systems by 17.32%, and 13.06%, respectively. From another perspective, using an insert for an unglazed PV/T system leads to considerable overall performance improvement (11.43%) compared to the base case with no mixing devices, while adding a glass cover makes the overall performance improvement a bit better (13.46%), at the penalty of additional weight and cost. Also, results show the insert reduces the spatial variation of cell temperature, which should reduce serious thermal stress and aging issues. To be commercially viable, the increase in cost and complexity of the PV/T module using a glass cover and/or wavy tape insert should be offset by the efficiency improvement; therefore, as a future recommendation, economic analysis for life cycle cost and cost payback for using a glass cover and/or wavy tape insert would be beneficial.

.References

Aleklett, K., Höök, M., Jakobsson, K., Lardelli, M., Snowden, S., Söderbergh, B., 2010. The peak of the oil age–analyzing the world oil production reference scenario in world energy outlook 2008. Energy Policy 38(3), 1398-1414.

Bellos, E., Tzivanidis, C., Tsimpoukis, D., 2017. Multi-criteria evaluation of parabolic trough collector with internally finned absorbers. Applied energy 205, 540-561.

Bhattarai, S., Oh, J.-H., Euh, S.-H., Kafle, G.K., Kim, D.H., 2012. Simulation and model validation of sheet and tube type photovoltaic thermal solar system and conventional solar collecting system in transient states. Solar Energy Materials and Solar Cells 103, 184-193.

Chow, T.T., Pei, G., Fong, K., Lin, Z., Chan, A., Ji, J., 2009. Energy and exergy analysis of photovoltaic–thermal collector with and without glass cover. Applied Energy 86(3), 310-316.

Comello, S., Reichelstein, S., Sahoo, A., 2018. The road ahead for solar PV power. Renewable and Sustainable Energy Reviews 92, 744-756.

Jaisankar, S., Ananth, J., Thulasi, S., Jayasuthakar, S.T., Sheeba, K.N., 2011. A comprehensive review on solar water heaters. Renewable and Sustainable Energy Reviews 15(6), 3045-3050.

Kazemian, A., Hosseinzadeh, M., Sardarabadi, M., Passandideh-Fard, M., 2018. Effect of glass cover and working fluid on the performance of photovoltaic thermal (PVT) system: An experimental study. Solar Energy 173, 1002-1010.

Kazemian, A., Khatibi, M., Reza Maadi, S., Ma, T., 2021. Performance optimization of a nanofluid-based photovoltaic thermal system integrated with nano-enhanced phase change material. Applied Energy, 116859.

Khanjari, Y., Pourfayaz, F., Kasaeian, A., 2016. Numerical investigation on using of nanofluid in a water-cooled photovoltaic thermal system. Energy Conversion and Management 122, 263-278.

Kolahan, A., Maadi, S.R., Kazemian, A., Schenone, C., Ma, T., 2020. Semi-3D transient simulation of a nanofluid-base photovoltaic thermal system integrated with a thermoelectric generator. Energy Conversion and Management 220, 113073.

Lu, Z., Yao, Q., 2007. Energy analysis of silicon solar cell modules based on an optical model for arbitrary layers. Solar Energy 81(5), 636-647.

Maadi, S.R., Khatibi, M., Ebrahimnia-Bajestan, E., Wood, D., 2019a. Coupled thermal-optical numerical modeling of PV/T module–Combining CFD approach and two-band radiation DO model. Energy Conversion and Management 198, 111781.

Maadi, S.R., Khatibi, M., Ebrahimnia-Bajestan, E., Wood, D., 2019b. Coupled thermal-optical numerical modeling of PV/T module – Combining CFD approach and two-band radiation DO model. Energy Conversion and Management 198, 111781.

Maadi, S.R., Khatibi, M., Ebrahimnia-Bajestan, E., Wood, D., 2019c. A parametric study of a novel PV/T system model which includes the greenhouse effect.

Maadi, S.R., Kolahan, A., Passandideh-Fard, M., Sardarabadi, M., Moloudi, R., 2017a. Characterization of PVT systems equipped with nanofluids-based collector from entropy generation. Energy Conversion and Management 150, 515-531.

Maadi, S.R., Kolahan, A., Passandideh Fard, M., Sardarabadi, M., 2017b. Effects of nanofluids thermo-physical properties on the heat transfer and 1st law of thermodynamic in a serpentine PVT system, Proceedings of the 17th Fluid Dynamics Conference, Shahrood, Iran. pp. 27-29.

Maadi, S.R., Navegi, A., Solomin, E., Ahn, H.S., Wongwises, S., Mahian, O., 2021. Performance Improvement of a Photovoltaic-Thermal System using a Wavy-strip Insert with and without nanofluids. Energy, 121190.

Maadi, S.R., Sabzali, H., Kolahan, A., Wood, D., 2020. Improving the performance of PV/T systems by using conical-leaf inserts in the coolant tubes. Solar Energy 212, 84-100.

Modest, M.F., 2013. Radiative heat transfer. Academic press.

Moradgholi, M., Nowee, S.M., Farzaneh, A., 2018. Experimental study of using Al 2 O 3 /methanol nanofluid in a two phase closed thermosyphon (TPCT) array as a novel photovoltaic/thermal system. Solar Energy 164, 243-250.

Sandeep, H., Arunachala, U., 2017. Solar parabolic trough collectors: A review on heat transfer augmentation techniques. Renewable and sustainable energy reviews 69, 1218-1231.

Sardarabadi, M., Hosseinzadeh, M., Kazemian, A., Passandideh-Fard, M., 2017. Experimental investigation of the effects of using metal-oxides/water nanofluids on a photovoltaic thermal system (PVT) from energy and exergy viewpoints. Energy 138, 682-695.

Skoplaki, E., Palyvos, J., 2009. On the temperature dependence of photovoltaic module electrical performance: A review of efficiency/power correlations. Solar energy 83(5), 614-624.

Appendix: Units and Symbols

Nomenclature

Quantity	Symbol	Unit
area	A	m^2
specific heat capacity	C_p	$J\,kg^{-1}K^{-1}$
power output	E	$W\,m^{-2}$
solar irradiance	G_{sun}	$W\,m^{-2}$
radiation intensity	I	$W\,m^{-2}$
thermal conductivity	k	$W\,m^{-1}K^{-1}$
mass flow rate	$\dot{m}$	$kg\,s^{-1}$
number of tubes	N	-
pressure	p	pa
packing factor	P_a	-
temperature	T	K
gravity	g	$m\,s^{-2}$
velocity	V	m/s

Greek symbols

Quantity	Symbol	Unit
reference temperature coefficient	β_{ref}	-
thermal expansion	β	-
efficiency	η	-
effective absorptance	$\bar{\alpha}$	-
transmittance	τ	-
scattering coefficient	σ_s	-
phase function	Φ	-
solid angle	Ω'	-
density	ρ	$kg\,m^{-3}$
difference	Δ	-
Absorptance	α	-
emissivity	ε	-
absorption coefficient	σ	m^{-1}
difference	Δ	-

Abbreviations

Preferred name	Symbol
Anti reflective coating	ARC
Discrete ordinate	DO
Ethylene vinyl acetate	EVA
Photovoltaic/thermal	PV/T
Photovoltaic	PV
Phase change material	PCM
Radiative transfer equation	RTE
Silicon	Si

Subscripts

Quantity	Symbol
absorption	a
ambient	amb
black body	b
fluid	f
electrical	$elec$
glass	g
inlet	in
overall	ov
outlet	out
photovoltaic	pv
pump	$pump$
reference	ref
sky	sky
solid	s
thermal	th
water	W
wind	$wind$
wavelength	λ